



Single-Source Thermal Ablation of halide perovskites, limitations and opportunities: The lesson of MAPbBr₃



Davide Calestani^{a,1}, Lucia Nasi^{a,1}, Francesco Mezzadri^{a,b}, Francesco Fracassi^{c,d},
Andrea Listorti^c, Patrizia Ferro^a, Roberto Mosca^{a,*}

^a CNR-IMEM Institute of Materials for Electronics and Magnetism, Parma, Italy

^b Department of Chemistry, Life Sciences and Environmental Sustainability, University of Parma, Parma, Italy

^c Department of Chemistry, University of Bari "Aldo Moro", Bari, Italy

^d CNR-NANOTEC Institute of Nanotechnology, c/o Department of Chemistry, University of Bari 'Aldo Moro', Bari, Italy

ARTICLE INFO

Article history:

Received 23 December 2020

Received in revised form 27 March 2021

Accepted 9 April 2021

Available online 15 April 2021

Keywords:

Flash evaporation

Halide perovskite

Thin film

CH₃NH₃PbBr₃

CsPbI₂Br

ABSTRACT

Single-Source Thermal Ablation (SSTA) is a vacuum-based evaporation method that was only minorly employed in the preparation of hybrid perovskite materials for solar cells despite some promising early achievements. We study the preparation of MAPbBr₃ films, showing that this material does not allow the reproducible preparation of thin films suitable for integration in multijunction devices due to the low adhesion of MABr to the substrate, on one hand, and to the proximity of decomposition and melting temperatures of MAPbBr₃ combined with the high vapor pressure of MABr on the other. Based on the insights obtained on MAPbBr₃ processing we demonstrate that, conversely, homogeneous fully-inorganic CsPbI₂Br thin films can be prepared by SSTA with a stability comparable to that reported for films obtained by spin coating. This work provides guidelines for the selection of halide perovskites that can be successfully prepared by SSTA for thin film application.

© 2021 Elsevier B.V. All rights reserved.

1. Introduction

Organic-inorganic metal-halide perovskites are currently considered a very interesting class of materials mainly because of their outstanding impact in solar cell application [1] that fostered also strong developments in perovskite-based optoelectronic applications exploiting not only thin films [2], but also nanocrystals [3,4]. Among PV applications, halide perovskites appear very appealing also for their potential exploitation in tandem with silicon to improve the performance of commercially available solar cells and reduce the cost of photovoltaic modules [5]. In most of these applications, poor morphology and bad substrate coverage limit the performance of the devices. In order to achieve smooth and pinhole-free films from solution methods, different approaches have been proposed [6,7]. Compared to solution-processing methods, vacuum evaporation naturally provides uniform and compact films with high reproducibility and fine thickness control, while offering integration

opportunities into complex devices such as monolithic tandem solar cells and LEDs. Most of the works on vacuum-based methods for ABX₃ halide perovskites exploit the dual source evaporation method [8–10], even if the use of different precursor vapors makes it difficult to keep control over the precursor ratio. Single-Source Thermal Ablation (SSTA, also named Flash Evaporation) is a simple alternative approach to the vacuum deposition of halide perovskites films, based on a single thermal source consisting in a metal foil heater used to vaporize rapidly the perovskite precursor by passing a large current. This method was used to prepare hybrid perovskites in the 1990s and 2000s for different applications [11,12], but in the recent season of halide perovskites for PVs, to the best of our knowledge, only very few works exploited this deposition technique. The first were Longo et al. [13], who performed the flash evaporation of MAPbI₃ in low vacuum (~0.1 mbar), obtaining films having a high degree of crystallinity and a smooth surface morphology. These films allowed power conversion efficiencies exceeding 12% in planar heterojunction solar cells. Later on, Xu et al. [14] showed that MAPbI₃ films prepared in of 0.1 mbar Ar pressure from stoichiometric precursors have pure perovskite phase but a rough surface with voids. On the contrary, film deposited under a low growth pressure of 5 10⁻⁵ mbar are dense and without pinholes, but PbI₂-free films can

* Corresponding author.

E-mail address: roberto.mosca@imem.cnr.it (R. Mosca).

¹ These authors have contributed equally to this work

only be achieved by using a precursor with an MAI-to-PbI₂ molar ratio of 2, which is necessary to compensate for the MAI loss during the transport of material from the source crucible to the substrate. They also showed that grain growth is limited by the presence of the PbI₂ phase in the films and obtained a ~10% maximum efficiency by using PbI₂-free films. Recently, the same group reported about the SSTA of formamidinium lead iodide (FAPI) [15], showing that PbI₂-free films can only be obtained by carrying out the deposition on substrates heated at 105 °C and using a FAI to PbI₂ molar ratio of 1.5 to compensate for the loss of FAI. The perovskite solar cell they obtained by using these films showed a 12.55% efficiency, but stability was lower than that of cells prepared by solution methods.

In spite of these rather promising results and the potential advantages deriving from being a relatively simple and quick process, SSTA was left behind without a clearly defined reason. Indeed, we recently showed that CsPbBr₃ films prepared by SSTA allow PeLED preparation, which confirms the suitability of SSTA for thin film application.

In this work we consider the deposition of MAPbBr₃ films by SSTA, showing that SSTA provides pure phase MAPbBr₃ films without any MABr excess sufficiently when high powers are used, but the proximity of the MAPbBr₃ decomposition and melting temperatures combined with the high vapor pressure of MABr produces spits on the film surface. Reduced power allows spit-free films, but requires the use of a MABr excess to compensate for the MABr losses during evaporation. This MABr excess yields pure phase MAPbBr₃ films, but at the cost of a significant loss of stability and reproducibility. These achievements point out that MAPbBr₃ films suitable for thin film application can hardly be obtained by SSTA. Based on the results obtained on MAPbBr₃ we demonstrate fully-inorganic CsPbI₂Br films which are instead suitable for applications such as light emitting devices and tandem solar cells.

2. Methods

Hybrid perovskite precursor solutions were prepared by using commercially available PbBr₂ (Aldrich), HI (57%) (Aldrich), and CH₃NH₂ (41% ethanol solution) (Fluka) without further purification. MABr was prepared by reacting amine solutions with HBr, as described previously [16]. In particular, methylamine (40% in water, Aldrich) was mixed with hydrobromic acid (48% in water, Aldrich) in a 1:1 molar ratio. After continuous stirring in the ice bath for 2 h, MABr was crystallized by removing the solvent at 65 °C for 2 h. The resultant precipitates, in the form of white crystals, were washed three times in diethyl ether, dried overnight under vacuum, and then stored in a dark, dry box.

MAPbBr₃ precursor solution (0.785 M) was prepared by stirring overnight at 60 °C equimolar mixtures of MABr and PbBr₂ in N,N-dimethylformamide (Fluka) and then naturally cooling down the solution, that appeared clear at room temperature. In order to achieve precursor solutions with a MAPbBr₃:MABr molar ratio of 1:x (0 ≤ x ≤ 2), proper amounts of MABr were added to the perovskite solution at room temperature while stirring.

For CsPbI₂Br films, a 0.45 M precursor solution was prepared by dissolving stoichiometric amounts of CsBr and PbBr₂ in dimethyl sulfoxide (Aldrich) at room temperature under stirring.

Glass substrates were cleaned by sequential rinsing in 1% Hellmanex, de-ionized water, hot acetone, and isopropanol for 15 min. After drying in blowing nitrogen, up to four substrates were placed on a sample holder that was mounted into the evaporation chamber at a fixed vertical distance from the evaporation source. The evaporation system was tailor made [12] following the schematization given by Mitzi et al. [11] and allowed power to be increased from 0 to the preset value with a rate of approximately 600 W/s, maximum power being 1000 W.

The precursor layer for evaporation was created by spreading 32 μl of the precursor solution onto a tantalum boat (Testbourne S46-.005Ta) that was then placed on a hotplate at 100 °C, while maintaining the precursor distribution as even as possible. For CsPbI₂Br 90 μl were used.

The boat was then clamped between two electrodes in the evaporation chamber that was immediately pumped to vacuum. When the pressure in the chamber was below 2 · 10⁻⁵ mbar, electrical current was passed through the boat to promote the precursor evaporation. Argon was finally inlet and samples removed from the chamber with the ambient humidity maintained below 30%. Unless stated otherwise, films were then stored into a desiccator in the dark.

Under these conditions, for a vertical distance of 8 cm between the crucible and the substrate, a film thickness of 240 nm was measured by a standard stylus profilometer.

When aiming to investigate the evolution of the evaporation process, deposition was performed in two steps: in the former one, a 90 W power preset was applied until the color of the precursor layer was seen to change from orange to whitish (step 1). The chamber was then opened, substrates were replaced by virgin others and the chamber was pumped again to vacuum. Then, a second evaporation was performed by applying the same 90 W power until the boat became incandescent (step 2).

Unless otherwise stated, all the film characterizations were carried out in low humidity atmosphere (RH ≤ 30%) after having aged the films for a few hours in desiccator. In particular, the structural quality of the films was studied by X-ray diffraction (XRD) measurements in a Siemens (D500) powder diffractometer, with CuK_α radiation. The refinement of XRD data was carried out using the GSAS II software [17].

Film absorbance spectra were measured by a Jasco UV-vis V-530 spectrometer. Morphological characterization was performed by atomic force microscopy using a Veeco Dimensions 3100 SPM and by scanning electron microscopy (SEM) using a Zeiss Auriga field emission microscope (FESEM) operated at 5 kV. Selected Area Electron Diffraction (SAED) and Energy Dispersive X-ray Spectrometry (EDS) were performed in a Jeol 2200FS Transmission Electron Microscope (TEM). To minimize any damage caused by the electron beam, the TEM measurements were carried out by using an acceleration voltage of 80 kV and a low beam current density.

Steady state and time resolved photoluminescence were measured by an Edinburgh FLS920 spectrometer equipped with a Peltier-cooled Hamamatsu R928 photomultiplier tube (185–850 nm). An Edinburgh Xe900 450 W Xenon arc lamp was used as exciting light source. Corrected spectra were obtained via a calibration curve supplied with the instrument (lamp power in the steady state PL experiments 0.6 mW cm⁻², spot area 0.5 cm²). Emission decay time were determined with the single photon counting technique by means of the same Edinburgh FLS980 spectrometer using a laser diode as excitation source (1 MHz, exc = 635 nm, 67 ps pulse width and about 30 ps time resolution after deconvolution) and a Hamamatsu MCP R3809U-50 (time resolution 20 ps) as detector. (Laser power in the TRPL experiment 1.6 W cm⁻², spot area 0.3 mm²) [18].

3. Results and discussion

In order to investigate the influence of the MABr excess, films were prepared using a power preset of 440 W. Unfortunately, the elemental composition could not be assessed by EDS because the Br/Pb ratio was found to rapidly drop upon electron irradiation, which limits the measurement accuracy. The XRD patterns of all the films are dominated by two peaks at 14.93° and 30.12°, respectively, (Fig. 1) corresponding to the 100 and 200 reflections of the MAPbBr₃ cubic phase [19]. However, pure phase films were achieved only

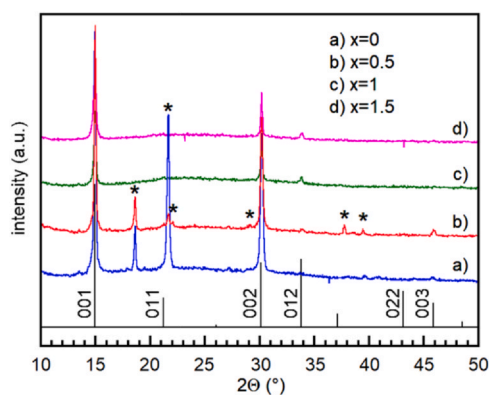


Fig. 1. XRD patterns of MAPbBr₃ films prepared by 440 W power preset with different MABr excesses. Stars indicate the PbBr₂ peaks. The reference pattern of MAPbBr₃ obtained from Ref. [19] is shown at the bottom.

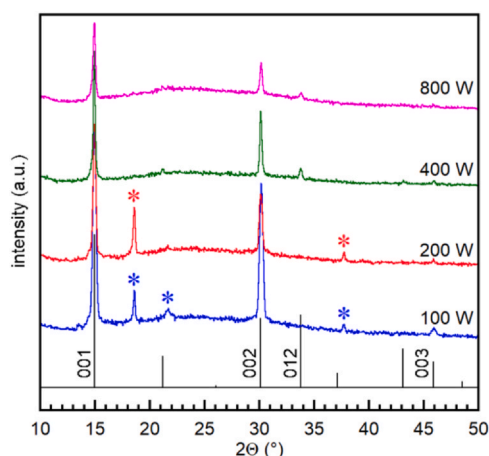


Fig. 2. XRD patterns of films obtained with (1:1) MAPbBr₃ to MABr molar ratio by using different power presets, as indicated. Stars indicate the PbBr₂ peaks. The reference pattern of MAPbBr₃ obtained from Ref. [19] is shown at the bottom.

when $x \geq 1$ was used, while for $x < 1$ peaks appear at 18.60° , 21.65° and 37.72° , that can be assigned to the 020, 120 and 040 reflections of the PbBr₂ orthorhombic phase, respectively (ICSD 202134). The observation that an excess of MABr is necessary to achieve pure phase films suggests that MABr is lost during evaporation. A similar result was reported for MAPbI₃ [14], where the same methylammonium halide excess was necessary to avoid the presence of PbI₂ phase in the perovskite films. In that case, a current of 180 A was considered high enough to yield the instantaneous evaporation of both PbI₂ and MAI. Based on the experimental details given in

Ref. [14], we infer that the power used in that case increased from ~ 48 W to ~ 130 W during evaporation. Here, when $x=1$ was used, pure phase MAPbBr₃ films were obtained only for power presets of at least 400 W (Fig. 2), while lower powers systematically produce PbBr₂ peaks in the XRD pattern. This means that, achieving pure phase MAPbBr₃ films requires a steeper temperature rise compared to MAPbI₃ [14], likely because of the higher vapor pressure of MABr.

Films obtained with $x=1$ and 400 W power preset show a compact and smooth surface with roughness of about 3.2 nm (Fig. 3A). The absorption spectra show an onset at ~ 535 nm (Fig. 3B) that is typical of MAPbBr₃ films prepared by spin coating [16,20]. The bandgap of ~ 2.33 eV determined by the Tauc plot may be considered in good agreement with the 2.31 eV value reported in the literature [16,20,21]. Indeed, the presence of interference fringes pointed out by the broad maximum at 590 nm, while confirming the good surface quality of the films, prevents a more accurate determination of the bandgap.

To rationalize how film properties would impact its optoelectronic performance, we recorded the steady state photoluminescence, measured its quantum yield (PLQY) and analyzed the PL decay (TRPL) of as-deposited perovskite films. The PL band is practically superimposed to the absorption band with minimum stoke shift. This is in line with what usually observed for MAPbBr₃ perovskites suggesting an emission from direct-gap recombination [22]. Noticeably, PLQY recorded at low excitation fluency, being 0.23% implies reasonably good optoelectronic properties of the material, as without special treatments polycrystalline film of MAPbBr₃ usually show PLQY below 1% [23]. Halide perovskites despite the straightforward deposition methodologies often exhibit superior optical properties than many other materials, but they still suffer from great loss of PL intensity and lifetime induced by trap-states. The emission decay time mirror what suggested by PLQY analysis as relatively long emission lifetime are retrieved. By fitting the PL decay with a multi-exponential decay law [24], we determine an average lifetime (τ) of 16.0 ns ($\tau_1 = 1.06$ ns, $\alpha_1 = 19.17$; $\tau_2 = 5.87$ ns, $\alpha_2 = 49.70$; $\tau_3 = 20.99$ ns, $\alpha_3 = 31.13$).

These results point out that film deposition performed by using a MABr excess of $x=1$ and a 400 W power preset provides good quality material. Unfortunately, we found that, except for the position of the absorbance onset, achieving an acceptable reproducibility of the film properties was a real issue, which forced us to investigate the evaporation process better. To this aim, we exploited a low power preset (90 W) to have a temperature rise slow enough to allow us to interrupt the deposition immediately after the orange precursor layer starts to change color to off-white. This way we found that at low powers the precursor decomposes so that the evaporation is made of two distinct steps: in the former one mainly MABr evaporates, while in the latter step, corresponding to the evaporation of the off-white layer, only PbBr₂ is deposited, in close similarity with what addressed for MAPbI₃ films [14]. Increasing the

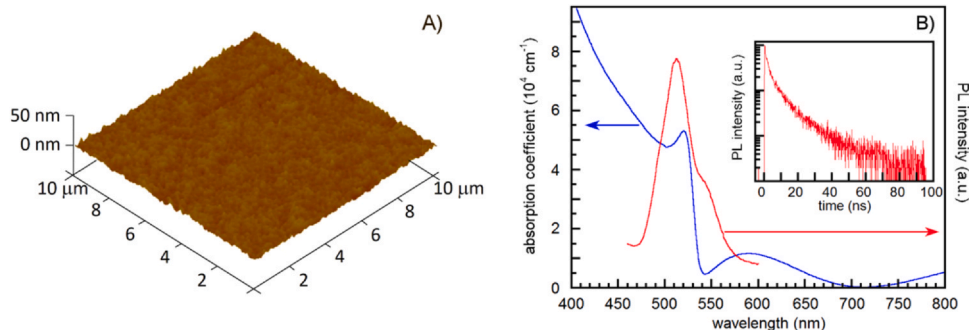


Fig. 3. Typical A) AFM image, B) absorbance and photoluminescence spectra (the relevant time-resolved PL decay is shown in the inset) of films prepared with (1:1) MABr-to-MAPbBr₃ molar ratio and a power preset of 400 W.

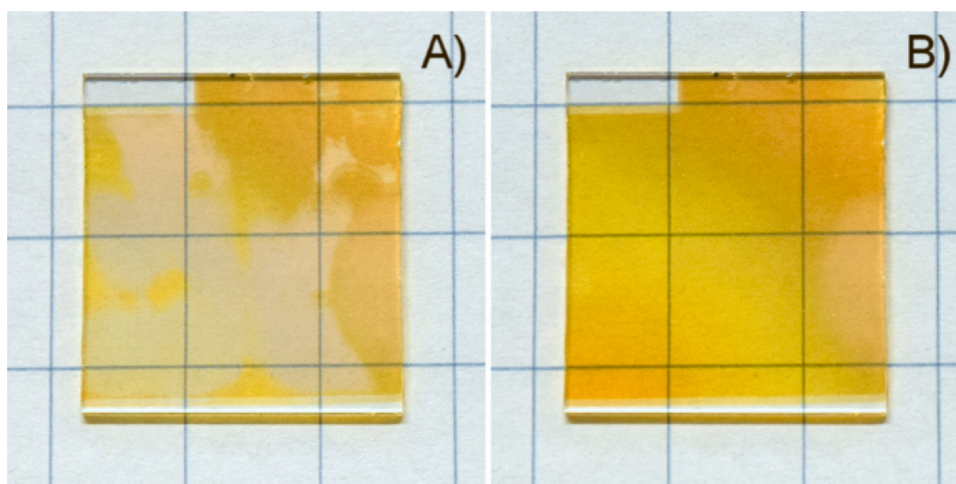


Fig. 4. Typical photographs of a film prepared by using a preset power of 440 W with a precursor containing a $x=1$ MABr excess (i.e. with a 1:1 MAPbBr₃:MABr molar ratio). Images were taken A) soon after extraction and B) after 20 min.

power preset makes the two steps gradually less distinct, so that at 400 W the formation of an off-white layer becomes less obvious than at low powers and is barely visible at 800 W. However, we cannot rule out that the MAPbBr₃ precursor decomposes at least partially even at high powers [25]. This two-step deposition process means that achieving pure phase MAPbBr₃ films requires that, after deposition, ion interdiffusion occur between the MABr-rich layers near the substrate and the PbBr₂-rich upper layers. Indeed, after their extraction from the deposition chamber films change color from pale yellow to orange in a few minutes through the formation of orange spots that appear soon after extraction and then extend up to cover the whole sample (Fig. 4). This evolution, that becomes more evident when the power preset is reduced and the MABr excess increased, is similar to the one observed in CsPbBr₃ films deposited by SSTA, where it was ascribed to a vertical composition gradient due to the precursor decomposition [25]. It is worth noting that this evolution takes place immediately after the exposure to ambient air, while keeping films in Ar or dry air flux for up to an hour before extraction did not prevent this evolution. This suggests that ambient humidity plays a role. Moisture is known to play a significant role during the formation of methylammonium lead halide perovskite films [26], although the details of involved mechanisms are still subject of debate [27]. In particular, water was proposed to enhance the reconstruction process during film formation by partially dissolving the reactants and accelerating mass transport within the film [28], while the exposure to humidity improves perovskite crystallinity [29].

We tried to investigate how this initial evolution affects the crystalline quality of the films. The XRD pattern of a film exposed to X-rays soon after deposition (Fig. 5) exhibits not only the peaks typical of the MAPbBr₃ cubic phase [19], but also peaks belonging to the PbBr₂ orthorhombic phase. On the contrary, PbBr₂ signatures were not observed on a film that, coming from the same deposition run, was kept for about two hours in the same RH = 30% atmosphere, but not exposed to X rays. In addition, soon after extraction the height of the XRD peaks of both perovskite and PbBr₂ change with time, whereas negligible pattern changes were observed under X-ray irradiation when measurements were performed after having stored films for 2–4 h in desiccator or in low humidity (RH ≤ 30%) atmosphere (Fig. 6A). These results highlight that X-ray irradiation interferes with the initial film evolution, which limits the possibility of studying the influence of the deposition parameters on the film crystallization soon after deposition as well as the initial evolution itself.

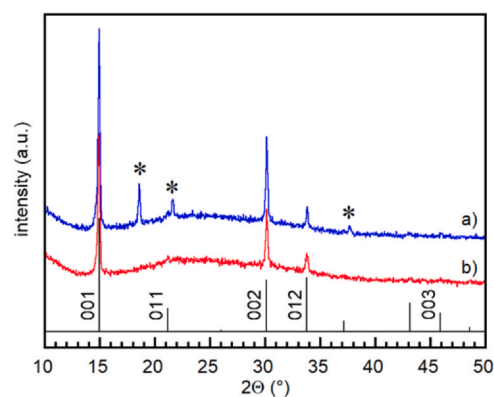


Fig. 5. XRD patterns of two films deposited in the same run (with $x=1$ and 440 W power preset). Films were exposed to X-rays for 30 min a) soon after extraction from the deposition chamber, b) after 2 h storage in the same atmosphere but in the dark. Relevant XRD measurements were performed immediately after this X-ray irradiation Stars point out peaks ascribed to PbBr₂. The reference pattern of MAPbBr₃ obtained from Ref. [19] is shown at the bottom.

The limited stability of as prepared films was confirmed by the observation that films placed under vacuum soon after extraction systematically show the presence of PbBr₂ (Fig. 6A, pattern c), likely connected to the formation of features (Fig. 6B) that are similar to the PbBr₂ clusters found in cleaved single crystals stored in vacuum for weeks [30]. The mechanism of PbBr₂ formation is likely the same proposed for MAPbI₃ films prepared by spin coating, where PbI₂ appears after 1 month vacuum storage due to the loss of volatile parts, likely HI and CH₃NH₂ [31]. Interestingly, twin samples prepared in the same deposition run do not exhibit PbBr₂ signatures after up to 14 days storage in desiccator (Fig. 6, patterns a and b). In addition, PbBr₂ formation was not observed in MAPbBr₃ films prepared by spin coating [16] that remain pure phase after more than one-year storage in vacuum (Fig. 6, pattern d). These results confirm that soon after extraction, films are prone to degradation likely due to the highly volatile and hygroscopic character of MABr. This means that the achievement of MAPbBr₃ films comes after an initial evolution phase that is influenced by not only the evaporation parameters (e.g. vacuum level, power preset) but also the environmental conditions the films experience during and immediately after its extraction from the evaporation chamber. This film delicacy is a real issue because it makes the extremely accurate control of both

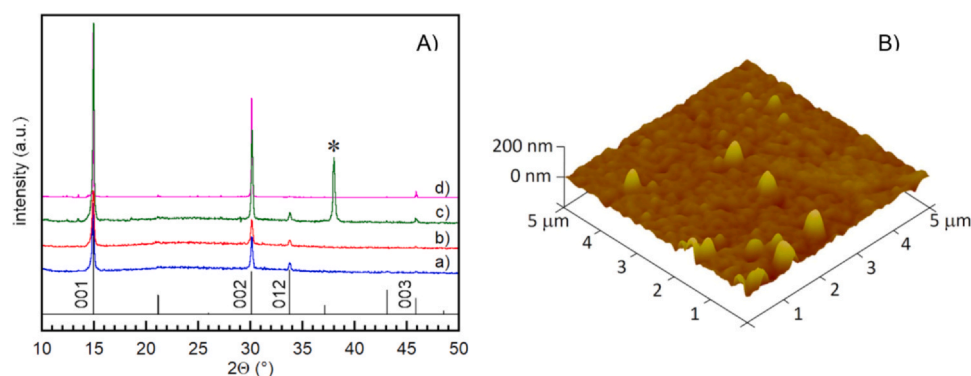


Fig. 6. A) XRD patterns of samples coming from the same deposition run as measured after a) 2 h storage in desiccator, b) 14 days in desiccator, and c) 2 days in vacuum. (the star indicates the 002 reflection of orthorhombic PbBr_2). Pattern d) refers to a film deposited by spin coating and measured after storage in vacuum for 390 days. The reference pattern of MAPbBr_3 obtained from Ref. [19] is shown at the bottom. B) AFM image taken on a film stored for 2 days in vacuum.

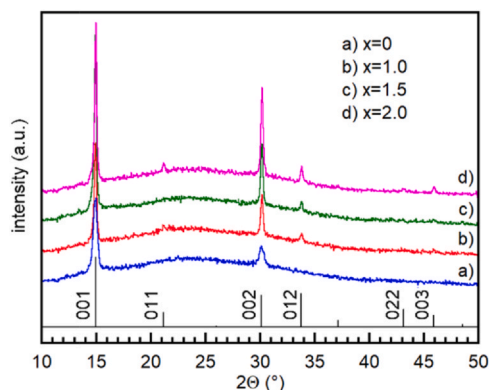


Fig. 7. XRD patterns of MAPbBr_3 films prepared at 800 W by using different MABr excesses, as indicated. The reference pattern of MAPbBr_3 obtained from Ref. [19] is shown at the bottom.

atmosphere and timings soon after extraction a prerequisite for achieving acceptable reproducibility of film properties.

Since the initial evolution comes from the vertical composition gradient due to the delay between MABr and PbBr_2 evaporation, we further increased power in order to reduce this delay. When a power preset of 800 W was used, the initial color change was not observed, while pure phase MAPbBr_3 films were obtained even for a stoichiometric precursors composition ($x=0$) (Fig. 7). This means that,

when power used is high enough, no MABr excess is necessary to achieve PbBr_2 -free films.

Unfortunately, while on the micrometric scale surface morphology appears flat and compact, similar to Fig. 3a, a larger view points out that bumps are present on the film surface with dimensions ranging from a few hundred nanometers to a few tens of micrometers (Fig. 8). EDS measurements performed on these bumps pointed out Br/Pb ratios that change with electron irradiation time, gradually approaching that of PbBr_2 . However, the same behavior was observed in the regions where the film is flat, which suggests that MAPbBr_3 perovskite films are unstable under an electron beam, as reported for MAPbBr_3 nanocrystals [32]. This instability hindered also TEM measurements, so that bump composition finally could not be assessed. Nevertheless, we observed that there is no correlation between the density and size of bumps and the presence of PbBr_2 in the XRD patterns, as we found bumps (Fig. 8B) even in films showing pure MAPbBr_3 perovskite phase (pattern c in Fig. 8F). Besides, we observed that bump density decreases with decreasing power (Fig. 8C-E), which suggests that these are MAPbBr_3 bumps likely due to spitting. Indeed, SSTA combines a rapid temperature rise, which is necessary to prevent the decomposition of the organic component, with high powers required to make PbBr_2 and MABr evaporations as simultaneous as possible. The rapid achievement of high temperatures is generally considered as one of the main causes of spitting because when the melting temperature is reached the molten precursor spreads over the crucible that continues heating very rapidly.

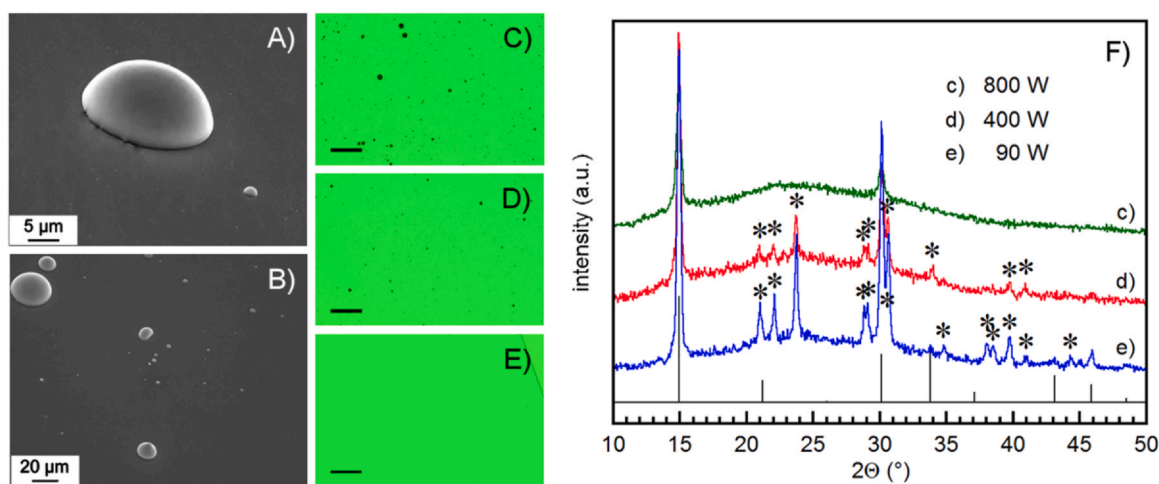


Fig. 8. A) and B) SEM images of bumps. C)–E) optical microscope images of film prepared without any MABr excess by using different power presets, namely C) 800 W, D) 400 W, and E) 90 W (markers indicate 250 μm). The relevant XRD patterns are shown in F) with the MAPbBr_3 reference pattern obtained from Ref. [19] (empty diamonds indicate PbBr_2 peak positions).

This creates vapor bubbles that can explode through the surface giving the spitting of molten material. Materials having high vapor pressures at their melting points are more likely to give spits [33]. In the present case, the formation of MAPbBr₃ spits can be justified considering that this material starts decomposing at ~220 °C [34]. While 3D lead perovskites are known to melt at temperatures near or above their decomposition temperature [6]. High heating rates are expected to shift the decomposition reaction to higher temperatures, so that decomposition and melting processes can overlap due to the fast crucible heating. Consequently, decomposition may take place in the presence of molten perovskite, which combined with the high vapor pressure of MABr may cause perovskite spits. This would be consistent with the observation that only the slow temperature raise obtained by power presets as small as 90 W prevents bump formation (Fig. 8D). Unfortunately, at these low powers the presence of PbBr₂ is unavoidable (pattern d in Fig. 8E), so that only a MABr excess of at least $x=2$ allows pure phase MAPbBr₃ films, which implies reduced film reproducibility and stability, as discussed above. The limited suitability for thin film application of MAPbBr₃ films obtained at high powers was confirmed by the lack of any electroluminescence in PeLEDs prepared by using these films.

We can conclude that this compound presents us with an insoluble problem, as the poor MABr adhesion on the substrate forces us to use high powers, that make films unsuitable for thin film application due to the spitting caused by the proximity of the decomposition temperature to the melting temperature, combined with the high vapor pressure of MABr. On the other hand, achieving pure phase MAPbBr₃ films by exploiting low powers to avoid spitting requires the use of MABr excesses that limit film stability, making reproducibility a real issue.

From the above results, we gather that, whenever the precursor compound does not sublime before decomposing, SSTA deposition starts with the decomposition of the perovskite precursor followed by the evaporation of the organic halide first and then of the lead halide. Although perovskite synthesis reaction is extremely favorable, achieving pure phase thin films becomes problematic if any of the evaporating species shows a low sticking coefficient while precursor decomposition temperature is close to the melting temperature, because of spitting phenomena, especially if any of the decomposition products has a high vapor pressure. This allows us to rationalize the preparation of CsPbBr₃ films by SSTA that we have previously reported [25]. Indeed, we obtained CsPbBr₃ films from stoichiometric precursors independently of the power used, confirming the absence of sticking problems for either PbBr₂ or CsBr. Besides, the melting temperature of CsPbBr₃ (567 °C) [35] is much larger than the decomposition one (450 °C) [36], which allowed us to take full advantage of the high evaporation rate of SSTA by increasing power while avoiding spitting, also because of the low vapor pressure of both CsBr and PbBr₂ compared to MABr.

Based on the achievements on MAPbBr₃ and CsPbBr₃, we infer that also CsPbI₂Br appears suitable to be prepared by SSTA since its melting temperature (463 °C) [37] is significantly higher than its decomposition temperature (330 °C) [38]. In addition, the vapor pressure of PbI₂ is only slightly larger than that of PbBr₂ [39] and we did not observe any adhesion issue. CsPbI₂Br combines the expected stability advantages deriving from the use of cesium in place of methylammonium cations with a great potential in tandem solar cell application due to the bandgap of about 1.9 eV [37]. For these reasons, we investigated the deposition of CsPbI₂Br films by SSTA. XRD patterns taken immediately after film extraction from the evaporation chamber show poor crystallization (Fig. 9A, pattern a), but, similar to what reported for CsPbI₂Br films prepared by solution methods [37,40], films turn dark brown after an annealing at temperatures larger than 250 °C. The surface of films annealed at 300 °C for 60 s appears compact and free of bumps, regardless of the power preset used (400 W in Fig. 9B).

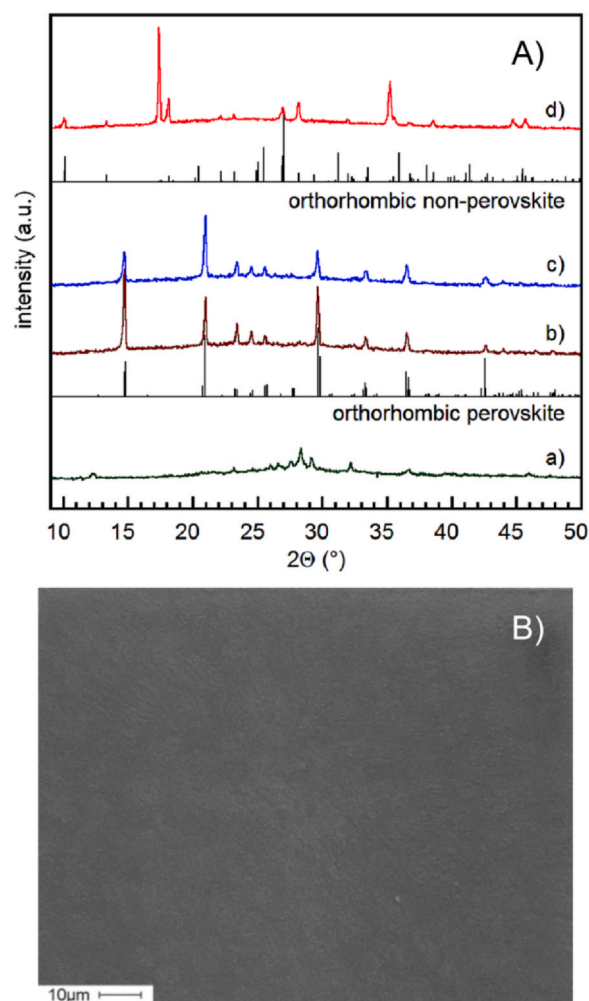


Fig. 9. (A) XRD patterns measured (a) soon after sample extraction from the deposition chamber, (b) soon after an annealing at 300 °C for 60 s (c) after having stored an annealed sample in desiccator for one month, and (d) after having exposed an annealed sample to ambient air (RH = 35%) for 180 min. The stick patterns for the orthorhombic perovskite and orthorhombic non-perovskite structures are also shown. (B) Typical SEM image of films deposited by SSTA at 400 W from the CsPbI₂Br precursor and annealed at 300 °C for 60 s.

The XRD patterns of freshly annealed brown films (Fig. 9A pattern b), despite being affected by (101) preferential orientation, are consistent with the orthorhombic perovskite polymorph of CsPbI₂Br [41]: Rietveld refinement of the PXRD data allowed us to determine the lattice parameters as $a=8.4873(19)$ Å, $b=11.981(6)$ Å, $c=8.558(2)$ Å. The SAED patterns (not shown) taken by scratching part of the brown film just before performing XRD, are in good agreement with the XRD patterns reported in Fig. 9A. Moreover, Quantitative EDS-TEM analysis showed that the Cs:Pb:I:Br is in good agreement with the 1:1:2:1 ratio, with a variation of about ± 2 atom % evaluated as the standard deviation in the fit. The EDS maps obtained in scanning TEM mode, shows a uniform distribution of Cs, Pb, I, and Br.

Absorbance spectra taken on brown films point out the presence of interference fringes (Fig. 10) that confirm the good surface quality of films. The absorbance onset at ~650 nm corresponds to a bandgap of 1.92 eV, as determined by the Tauc plot, that is in good agreement with the value reported for CsPbI₂Br thin films prepared by spin coating [37,40]. The above results confirm that SSTA provides good quality CsPbI₂Br films.

We finally assessed the stability of the films obtained by SSTA, because the CsPbI₂Br brown perovskite phase, although used in PV

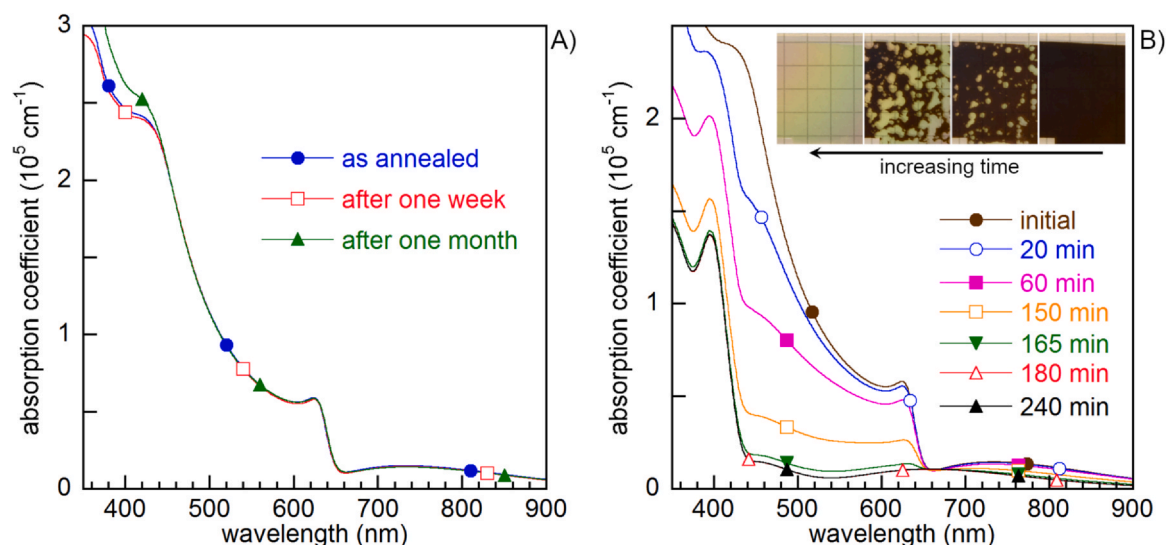


Fig. 10. Absorbance spectra of films annealed at 300 °C for 1 min (A) spectra measured either soon after annealing or after storage in desiccator, as indicated; (B) spectra measured after exposure to ambient air (RH = 35%) for times indicated. The inset shows the conversion from the brown phase to the yellow one for a CsPbI₂Br film exposed to ambient air (RH = 35%).

applications, is known to be metastable at room temperature, the thermodynamically stable structure being an orthorhombic non-perovskite structure (yellow phase). After having stored the film in desiccator for up to one month, we found that the XRD pattern of the aged film is consistent with the just annealed one (Fig. 9A, pattern b and c). Besides, storing films in desiccator for up to one month does not affect significantly its absorbance spectrum (Fig. 10A), whereas exposing the film to ambient air progressively decreases its absorbance at a rate that depends on humidity. Indeed, in RH \leq 27% the absorption intensity at the peak of onset (624 nm) decreases by less than 0.5% after 120 min, whereas at RH \sim 35% the decrease is already \sim 3.5% after 20 min and continues until the perovskite absorbance step completely disappears after about 3 h (Fig. 10B). During the exposure to ambient air, pale spots appear and then increase in size to cover the entire film (inset in Fig. 10B). After the color change has come to completion, in addition to interference fringes the absorbance spectrum points out a step at \sim 430 nm, that corresponds to a 2.94 eV bandgap, as obtained from the Tauc plot. The XRD pattern of converted films (Fig. 10 pattern d) is consistent with a [100] oriented orthorhombic non perovskite phase [42] having lattice parameters $a = 10.191(2) \text{ \AA}$ $b = 5.016(3) \text{ \AA}$ $c = 17.462(12) \text{ \AA}$, thus confirming that the brown phase has converted to the yellow one. This behavior is fully consistent with what previously reported for CsPbI₂Br films obtained by spin coating [37], which points out that SSTA allows us to obtain CsPbI₂Br films that are not only suitable for thin film application, but also have stability properties comparable to those of films obtained by solution methods.

This first demonstration of CsPbI₂Br films obtained by SSTA confirms that the high deposition rate of this technique can be fully exploited for thin film application when 1) the decomposition and melting temperatures of the precursor material are not close to each other and 2) the decomposition products have relatively low vapor pressure. This allows us to raise some doubts on the efficacy of SSTA for MA-based halide perovskites, but at the same time to envisage the suitability of the SSTA technique for the preparation of fully inorganic halide perovskite thin films.

4. Conclusions

We have investigated the preparation of hybrid MAPbBr₃ perovskite films by SSTA, showing that sufficiently high powers allow for pure phase films withstanding no MABr excess. However, high

powers produce MAPbBr₃ spits on the film surface, thus hindering their thin film application. Spitting is due to the proximity of the decomposition and melting temperatures, combined with the high vapor pressure of MABr. Using intermediate powers allows stoichiometric films to be obtained only when a precursor containing a proper MABr excess is used, but the presence of an initial evolution makes these films prone to degradation, while spits persist. Low powers yield spit-free films, but pure phase MAPbBr₃ cannot be achieved even by increasing the MABr excess to $x = 2$, which, in turn, affects reproducibility and stability. Therefore, the combination of the delay between MABr and PbBr₂ evaporation, the poor MABr adhesion on the substrate, the proximity of the MAPbBr₃ decomposition and melting temperatures, and the high vapor pressure of MABr prevents us from obtaining by SSTA pure phase MAPbBr₃ films suitable for thin film application. Based on these results, we have however rationalized that CsPbBr₃ films can be successfully prepared by SSTA because the decomposition and melting temperatures are far enough, while the decomposition products (CsBr and PbBr₂) have low enough vapor pressures and do not show sticking problems. Moving from this analysis, for the first time we successfully applied SSTA to CsPbI₂Br achieving films that not only are suitable for thin film application, but have also a stability comparable to that of films of the same material prepared by solution methods. These results shine new light on the SSTA technique for the preparation of fully inorganic halide perovskite thin films.

CRediT authorship contribution statement

Davide Calestani: Validation, Investigation, Writing - Review & Editing. **Lucia Nasi:** Validation, Investigation, Writing - Review & Editing. **Francesco Mezzadri:** Investigation, Writing - Review & Editing. **Francesco Fracassi:** Writing - Review & Editing. **Andrea Listorti:** Investigation, Writing - Review & Editing. **Patrizia Ferro:** Investigation, Resources. **Roberto Mosca:** Validation, Investigation, Writing - Original Draft, Writing - Review & Editing, Supervision.

Declaration of Competing Interest

The authors declare that they have no known competing financial interests or personal relationships that could have appeared to influence the work reported in this paper.

Acknowledgments

LN, DC, FM, PF, and RM thank T. Besagni for technical assistance. Thanks are due to M. Mazzeo for his availability in the preparation of PeLEDs. The work was supported by the project entitled "Tecnologia per celle solari bifacciali ad alta Efficienza a 4 terminali per utility scale" (BEST4U), Research Project ARS01_00519 funded under the PON "R&I" 2014-2020 Program - Action II - D.D. Prot. N. 2059 of 02/08/2018, financed by the Italian Ministry MUR.

References

- [1] J.Y. Kim, J.W. Lee, H.S. Jung, H. Shin, N.G. Park, High-efficiency perovskite solar cells, *Chem. Rev.* 120 (2020) 7867–7918, <https://doi.org/10.1021/acs.chemrev.0c00107>
- [2] H. Cho, C. Wolf, J.S. Kim, H.J. Yun, J.S. Bae, H. Kim, J.M. Heo, S. Ahn, T.W. Lee, High-efficiency solution-processed inorganic metal halide perovskite light-emitting diodes, *Adv. Mater.* 29 (2017), <https://doi.org/10.1002/adma.201700579>
- [3] G. Qiao, Z. Zeng, J. Gao, Y. Tang, Q. Wang, An efficient route to assemble novel organometal halide perovskites and emission evolution performance, *J. Alloy. Compd.* 771 (2019) 418–423, <https://doi.org/10.1016/j.jallcom.2018.08.322>
- [4] X. Liu, J. Gao, W. Liu, Q. Wang, Reinforcing effects of waterproof substrate on the photo-, thermal and pH stabilities of perovskite nanocrystals, *J. Alloy. Compd.* 817 (2020) 152693, <https://doi.org/10.1016/j.jallcom.2019.152693>
- [5] J. Werner, B. Niesen, C. Ballif, Perovskite/silicon tandem solar cells: marriage of convenience or true love story? – An overview, *Adv. Mater. Interfaces* 5 (2018) 1–19, <https://doi.org/10.1002/admi.201700731>
- [6] W.A. Dunlap-Shohl, Y. Zhou, N.P. Padture, D.B. Mitzi, Synthetic approaches for halide perovskite thin films, *Chem. Rev.* 119 (2019) 3193–3295, <https://doi.org/10.1021/acs.chemrev.8b00318>
- [7] A. Giuri, S. Masi, A. Listorti, G. Gigli, S. Colella, C. Esposito Corcione, A. Rizzo, Polymeric rheology modifier allows single-step coating of perovskite ink for highly efficient and stable solar cells, *Nano Energy* 54 (2018) 400–408, <https://doi.org/10.1016/j.nanoen.2018.10.039>
- [8] L.K. Ono, M.R. Leyden, S. Wang, Y. Qi, Organometal halide perovskite thin films and solar cells by vapor deposition, *J. Mater. Chem. A* 4 (2016) 6693–6713, <https://doi.org/10.1039/c5ta08963h>
- [9] M. Sessolo, C. Mombiona, L. Gil-Escrig, H.J. Bolink, Photovoltaic devices employing vacuum-deposited perovskite layers, *MRS Bull.* 40 (2015) 660–666, <https://doi.org/10.1557/mrs.2015.170>
- [10] F. Mariano, A. Listorti, A. Rizzo, S. Colella, G. Gigli, M. Mazzeo, Thermally evaporated hybrid perovskite for hetero-structured green light-emitting diodes, *Appl. Phys. Lett.* 111 (2017) 163301, <https://doi.org/10.1063/1.5001828>
- [11] D.B. Mitzi, M.T. Prikas, K. Chondroudis, Thin film deposition of organic-inorganic hybrid materials using a single source thermal ablation technique, *Chem. Mater.* 11 (1999) 542–544, <https://doi.org/10.1021/cm9811139>
- [12] R. Mosca, P. Ferro, T. Besagni, D. Calestani, F. Chiarella, F. Licci, Effect of humidity on the a.c. Impedance of $\text{CH}_3\text{NH}_3\text{SnCl}_3$ hybrid films, *Appl. Phys. A Mater. Sci. Process.* 104 (2011) 1181–1187, <https://doi.org/10.1007/s00339-011-6407-z>
- [13] G. Longo, L. Gil-Escrig, M.J. Degen, M. Sessolo, H.J. Bolink, Perovskite solar cells prepared by flash evaporation, *Chem. Commun.* 51 (2015) 7376–7378, <https://doi.org/10.1039/c5cc01103e>
- [14] H. Xu, Y. Wu, F. Xu, J. Zhu, C. Ni, W. Wang, F. Hong, R. Xu, F. Xu, J. Huang, L. Wang, Grain growth study of perovskite thin films prepared by flash evaporation and its effect on solar cell performance, *RSC Adv.* 6 (2016) 48851–48857, <https://doi.org/10.1039/c6ra07549e>
- [15] F. Xu, Y. Tian, W. Wang, Y. Zhu, L. Zeng, B. Yao, Z. Fang, H. Xu, R. Xu, F. Xu, F. Hong, L. Wang, In situ deposition of black α -FAPbI₃ films by vacuum flash evaporation for solar cells, *J. Mater. Sci. Mater. Electron.* 30 (2019) 8381–8389, <https://doi.org/10.1007/s10854-019-01155-w>
- [16] P. Fedeli, F. Gazza, D. Calestani, P. Ferro, T. Besagni, A. Zappettini, G. Calestani, E. Marchi, P. Ceroni, R. Mosca, Influence of the synthetic procedures on the structural and optical properties of mixed-halide (Br, I) perovskite films, *J. Phys. Chem. C* 119 (2015) 21304–21313, <https://doi.org/10.1021/acs.jpcc.5b03923>
- [17] B.H. Toby, R.B. Von Dreele, GSAS-II: the genesis of a modern open-source all purpose crystallography software package, *J. Appl. Crystallogr.* 46 (2013) 544–549, <https://doi.org/10.1107/S0021889813003531>
- [18] S. Masi, F. Aiello, A. Listorti, F. Balzano, D. Altamura, C. Giannini, R. Caliendo, G. Uccello-Barretta, A. Rizzo, S. Colella, Connecting the solution chemistry of PbI₂ and MAI: a cyclodextrin-based supramolecular approach to the formation of hybrid halide perovskites, *Chem. Sci.* 9 (2018) 3200–3208, <https://doi.org/10.1039/c7sc05095j>
- [19] H. Mashiyama, Disordered cubic perovskite structure of $\text{CH}_3\text{NH}_3\text{PbX}_3$ (X = Cl, Br, I), *J. Korean Phys. Soc.* 32 (1998) S156–S158 (<https://www.jkps.or.kr/journal/view.html?uid=2518&vmd=Full>)
- [20] X. Zheng, B. Chen, C. Wu, S. Priya, Room temperature fabrication of $\text{CH}_3\text{NH}_3\text{PbBr}_3$ by anti-solvent assisted crystallization approach for perovskite solar cells with fast response and small J-V hysteresis, *Nano Energy* 17 (2015) 269–278, <https://doi.org/10.1016/j.nanoen.2015.08.023>
- [21] H.M. Kim, Y.C. Kim, H.J. An, J.M. Myoung, Highly stretchable and contact-responsive light-emitting diodes based on MAPbBr₃-PEO composite film, *J. Alloy. Compd.* 819 (2020) 153360, <https://doi.org/10.1016/j.jallcom.2019.153360>
- [22] Z.Y. Zhang, H.Y. Wang, Y.X. Zhang, Y.W. Hao, C. Sun, Y. Zhang, B.R. Gao, Q.D. Chen, H.B. Sun, The role of trap-assisted recombination in luminescent properties of organometal halide $\text{CH}_3\text{NH}_3\text{PbBr}_3$ perovskite films and quantum dots, *Sci. Rep.* 6 (2016) 1–7, <https://doi.org/10.1038/srep27286>
- [23] K. Lin, J. Xing, L.N. Quan, F.P.G. de Arquer, X. Gong, J. Lu, L. Xie, W. Zhao, D. Zhang, C. Yan, W. Li, X. Liu, Y. Lu, J. Kirman, E.H. Sargent, Q. Xiong, Z. Wei, Perovskite light-emitting diodes with external quantum efficiency exceeding 20 per cent, *Nature* 562 (2018) 245–248, <https://doi.org/10.1038/s41586-018-0575-3>
- [24] J.R. Lakowicz, *Principles of Fluorescence Spectroscopy*, 3rd ed., Springer, US, 2006.
- [25] L. Nasi, D. Calestani, F. Mezzadri, F. Mariano, A. Listorti, P. Ferro, M. Mazzeo, R. Mosca, All-Inorganic CsPbBr₃ perovskite films prepared by single source thermal ablation, *Front. Chem.* 8 (1–10) (2020) 313, <https://doi.org/10.3389/fchem.2020.00313>
- [26] G.E. Eperon, S.N. Habisreutinger, T. Leijtens, B.J. Bruijnaers, J.J. Van Franeker, D.W. Dequillettes, S. Pathak, R.J. Sutton, G. Grancini, D.S. Ginger, R.A.J. Janssen, A. Petrozza, H.J. Snaith, The importance of moisture in hybrid lead halide perovskite thin film fabrication, *ACS Nano* 9 (2015) 9380–9393, <https://doi.org/10.1021/acsnano.5b03626>
- [27] A. Dubey, N. Adhikari, S. Mabrouk, F. Wu, K. Chen, S. Yang, Q. Qiao, A strategic review on processing routes towards highly efficient perovskite solar cells, *J. Mater. Chem. A* 6 (2018) 2406–2431, <https://doi.org/10.1039/c7ta08277k>
- [28] H. Zhou, Q. Chen, G. Li, S. Luo, T.-B. Song, H.-S. Duan, Z. Hong, J. You, Y. Liu, Y. Yang, Interface engineering of highly efficient perovskite solar cells, *Science* (80-) 345 (2014) 542–546, <https://doi.org/10.1126/science.1254050>
- [29] K.K. Bass, R.E. McAnally, S. Zhou, P.I. Djurovich, M.E. Thompson, B.C. Melot, Influence of moisture on the preparation, crystal structure, and photophysical properties of organohalide perovskites, *Chem. Commun.* 50 (2014) 15819–15822, <https://doi.org/10.1039/c4cc005231e>
- [30] J.I. Choi, M.E. Khan, Z. Hawash, K.J. Kim, H. Lee, L.K. Ono, Y. Qi, Y.H. Kim, J.Y. Park, Atomic-scale view of stability and degradation of single-crystal MAPbBr₃ surfaces, *J. Mater. Chem. A* 7 (2019) 20760–20766, <https://doi.org/10.1039/c9ta05883d>
- [31] I. Deretzis, A. Aliberti, G. Pellegrino, E. Smecca, F. Giannazzo, N. Sakai, T. Miyasaka, A. La Magna, Atomistic origins of $\text{CH}_3\text{NH}_3\text{PbI}_3$ degradation to PbI₂ in vacuum, *Appl. Phys. Lett.* 106 (2015) 3–8, <https://doi.org/10.1063/1.4916821>
- [32] F. Zhu, L. Men, Y. Guo, Q. Zhu, U. Bhattacharjee, P.M. Goodwin, J.W. Petrich, E.A. Smith, J. Vela, Shape evolution and single particle luminescence of organometal halide perovskite nanocrystals, *ACS Nano* 9 (2015) 2948–2959, <https://doi.org/10.1021/nn507020s>
- [33] D.M. Mattox, *Handbook of Physical Vapor Deposition (PVD) Processing*, 2nd ed., Elsevier, United Kingdom, 2010, <https://doi.org/10.1016/B978-0-8155-2037-5.00025-3>
- [34] M. Kulbak, S. Gupta, N. Kedem, I. Levine, T. Bendikov, G. Hodes, D. Cahen, Cesium enhances long-term stability of lead bromide perovskite-based solar cells, *J. Phys. Chem. Lett.* 7 (2016) 167–172, <https://doi.org/10.1021/acs.jpcclett.5b02597>
- [35] C. Zhang, J.F.S. Fernando, K.L. Firestein, J.E. Von Treifeldt, D. Siriwardena, X. Fang, D. Golberg, Thermal stability of CsPbBr₃ perovskite as revealed by in situ transmission electron microscopy, *APL Mater.* 7 (2019) 1–7, <https://doi.org/10.1063/1.5108849>
- [36] M. Liao, B. Shan, M. Li, In situ Raman spectroscopic studies of thermal stability of all-inorganic cesium lead halide (CsPbX₃, X=Cl, Br, I) perovskite nanocrystals, *J. Phys. Chem. Lett.* 10 (2019) 1217–1225, <https://doi.org/10.1021/acs.jpcclett.9b00344>
- [37] S. Mariotti, O.S. Hutter, L.J. Phillips, P.J. Yates, B. Kundu, K. Durose, Stability and performance of CsPbI₂Br thin films and solar cell devices, *ACS Appl. Mater. Interfaces* 10 (2018) 3750–3760, <https://doi.org/10.1021/acsami.7b14039>
- [38] J.K. Nam, M.S. Jung, S.U. Chai, Y.J. Choi, D. Kim, J.H. Park, Unveiling the crystal formation of cesium lead mixed-halide perovskites for efficient and stable solar cells, *J. Phys. Chem. Lett.* 8 (2017) 2936–2940, <https://doi.org/10.1021/acs.jpcclett.7b01067>
- [39] J.G. Speight, Chapter Four - Properties of Inorganic Compounds, in: J.G. Speight (Ed.), *Environ. Inorg. Chem. Eng. Butterworth-Heinemann*, 2017, pp. 171–229, <https://doi.org/10.1016/B978-0-12-849891-0.00004-7>
- [40] R.J. Sutton, G.E. Eperon, L. Miranda, E.S. Parrott, B.A. Kamino, J.B. Patel, M.T. Hörantner, M.B. Johnston, A.A. Haghighirad, D.T. Moore, H.J. Snaith, Bandgap-tunable cesium lead halide perovskites with high thermal stability for efficient solar cells, *Adv. Energy Mater.* 6 (2016) 1–6, <https://doi.org/10.1002/aenm.201502458>
- [41] C.C. Stoumpos, C.D. Malliakas, J.A. Peters, Z. Liu, M. Sebastian, J. Im, T.C. Chasapis, A.C. Wibowo, D.Y. Chung, A.J. Freeman, B.W. Wessels, M.G. Kanatzidis, Crystal growth of the perovskite semiconductor CsPbBr₃: a new material for high-energy radiation detection, *Cryst. Growth Des.* 13 (2013) 2722–2727, <https://doi.org/10.1021/cg400645t>
- [42] D.M. Trots, S.V. Myagkota, High-temperature structural evolution of caesium and rubidium triiodoplumbates, *J. Phys. Chem. Solids* 69 (2008) 2520–2526, <https://doi.org/10.1016/j.jpcs.2008.05.007>